remote sensing

MDPI

Article

Remote Sensing of Sea Surface Artificial Floating Plastic Targets with Sentinel-2 and Unmanned Aerial Systems (Plastic Litter Project 2019)

Konstantinos Topouzelis [1,*], Dimitris Papageorgiou [1], Alexandros Karagaitanakis [1], Apostolos Papakonstantinou [1] and Manuel Arias Ballesteros [2]

1 Department of Marine Science, University of the Aegean, University Hill, 81100 Mytilene, Greece; d.papageorgiou@aegean.gr (D.P.); mar15032@marine.aegean.gr (A.K.); apapak@aegean.gr (A.P.)
2 Argans Ltd., Chamberlain House, 1 Research Way, Plymouth PL6 8BU, UK; marias@argans.co.uk
* Correspondence: topouzelis@marine.aegean.gr; Tel.: +30-2251036878

Received: 3 May 2020; Accepted: 21 June 2020; Published: 23 June 2020

check for updates

Abstract: Remote sensing is a promising tool for the detection of floating marine plastics offering extensive area coverage and frequent observations. While floating plastics are reported in high concentrations in many places around the globe, no referencing dataset exists either for understanding the spectral behavior of floating plastics in a real environment, or for calibrating remote sensing algorithms and validating their results. To tackle this problem, we initiated the Plastic Litter Projects (PLPs), where large artificial plastic targets were constructed and deployed on the sea surface. The first such experiment was realised in the summer of 2018 (PLP2018) with three large targets of 10 × 10 m. Hereafter, we present the second Plastic Litter Project (PLP2019), where smaller 5 × 5 m targets were constructed to better simulate near-real conditions and examine the limitations of the detection with Sentinel-2 images. The smaller targets and the multiple acquisition dates allowed for several observations, with the targets being connected in a modular way to create different configurations of various sizes, material composition and coverage. A spectral signature for the PET (polyethylene terephthalate) targets was produced through modifying the U.S. Geological Survey PET signature using an inverse spectral unmixing calculation, and the resulting signature was used to perform a matched filtering processing on the Sentinel-2 images. The results provide evidence that under suitable conditions, pixels with a PET abundance fraction of at least as low as 25% can be successfully detected, while pinpointing several factors that significantly impact the detection capabilities. To the best of our knowledge, the 2018 and 2019 Plastic Litter Projects are to date the only large-scale field experiments on the remote detection of floating marine litter in a near-real environment and can be used as a reference for more extensive validation/calibration campaigns.

Keywords: plastic marine litter; marine debris; UAS; Sentinel-2; matched filtering

1. Introduction

Floating marine plastics are a threatening problem for the world's oceans. An increasing number of scientific publications evidence the issue [1,2]. Several studies aim to tackle the problem with information derived from observers on a cruise [3], the use of modeling [4–9], and remote sensing [10–12]. The need for an integrated marine debris observing system was presented by Maximenko et al. [13], while directions on the detection requirements are given by international groups and agencies [13–18].

Remote sensing is one of the tools necessary for the detection of floating marine plastics because of the extensive area coverage and frequent observation. An initial assessment of the observation requirements for measuring marine plastics from space was given by Martínez-Vicente et al. [11].

Although the remote sensing detection algorithms are immature, several studies have been working in this direction on optical and thermal modeling [19,20], on hyperspectral modeling and analysis [21–24], on drones or stable cameras [25–31], and with the direct use of satellite imagery [10,12,32]. Additionally, the use of marine floating indices derived from satellite images could offer a valuable monitoring tool [33–35].

While floating plastics are reported in high concentrations in many places around the globe, no referencing dataset exists either for understanding the spectral behavior of plastics in the real environment, or for calibrating remote sensing algorithms and validating their results. To tackle this problem, we decided to construct large artificial targets and to deploy them on the sea surface. The Plastic Litter Project (PLP) was first conducted in 2018 (PLP2018) as an explorative feasibility study on the detection of floating plastics in the aquatic environment using data acquired from unmanned aerial systems (UAS) and open-access satellite missions [10]. The project objective was to examine the visibility of the plastic targets from the Copernicus Sentinel-2 satellite and to simulate the coarse satellite pixel using the fine UAS resolution.

Hereafter, we present the second Plastic Litter Project, which was conducted in the summer of 2019 (PLP2019, all data can be found in Appendix A). The PLP2019 was scheduled for a two-month field campaign (May–June 2019), with 13 scheduled Sentinel-2 acquisition dates. Smaller targets were created in order to be closer to reality and to examine the limitations of the detection with Sentinel-2 images. The smaller targets and the multiple measurements allowed several observations, since the targets were connected in a modular way to create new configurations of different sizes, material composition and plastic coverage. To the best of our knowledge, the 2018 and 2019 Plastic Litter Projects are so far the only large-scale field experiments on the remote detection of floating marine litter in a near-real environment. The PLPs can be used as a reference for scaling up the validation/calibration campaigns for floating marine litter detection.

2. Materials and Methods

2.1. Targets Description

Two new types of targets were created for the PLP2019; one with 5×5 m size and one with 1×5 m size. With the first type, we were able to make several configurations on the sea surface and simulate different sizes and shapes, while with the second type we wanted to examine the detection limitations of elongated plastic targets, which simulate the litter windrows found in a real environment. Six targets were created for the first type and two targets for the second type. The targets consisted of PVC pipes with a 5 cm diameter, and in the 5×5 m targets, a cross bracing was used to strengthen the structure (Figure 1). On the cross center, we created a GPS housing and we mounted a GPS to get the exact location of the targets. This was the first time a GPS was included in the Plastic Litter Projects and it was found to be very efficient in cross-checking the position of the targets. Also, a plastic mesh with a 1.5 cm mesh size was attached to the frames as a base. The frame and the net were essential to prevent plastic loss in the sea.

The materials of the targets were 1.5-liter clear PET bottles (PET-1, polyethylene terephthalate), plastic bags (low-density polyethylene, LDPE), and in one case natural debris (reeds, *Arundo donax)*. Each PET target consisted of 416 bottles (26 lines with 16 bottles each), and a nylon rope that was threaded through the bottom of the bottle and the bottle cap. PET bottles were used as a target material as they can be regularly observed floating in busy coastal waters and harbors, especially in touristic areas. In addition, PET bottles are a clean and easy to work with material that reduces chances of water contamination. The plastic bags targets consisted of large blue plastic bags, typical of household wastes, and they were attached to the PVC frame using nylon rope (Figure 1).

The targets were deployed into the water every five days, synchronized with Sentinel-2 acquisitions, and were removed after the satellite overpass. The site of the field experiments was the same as for PLP2018 [10], in the coastal waters of the island of Lesvos in Greece, in the vicinity of Tsamakia Beach in Mytilene. To simulate open water optical conditions, an effort was made to set the targets above seagrass meadows (*Posidonia oceanica*). This was decided in order to minimize the signal contribution of an otherwise bright seafloor, due to light-colored sediments.

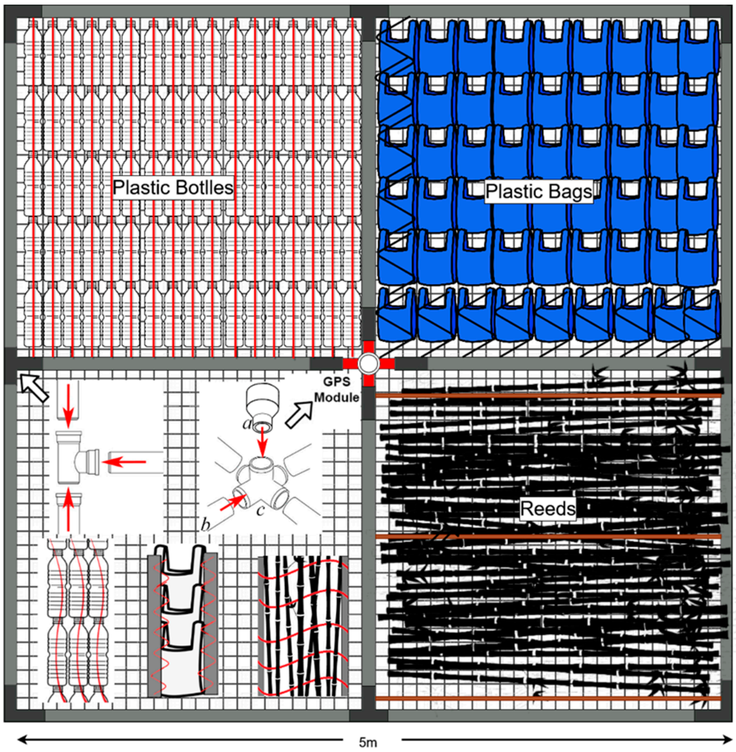

Figure 1. Schematic representation of the 5 × 5 m plastic target with the different materials used as reference debris. For schematic purposes each quadrant presents the way of the litter placement in a full target. The fourth quadrant illustrates the connection of the frame and the litter attachment.

Configurations and Plastic Coverage

The small size of the targets was convenient to generate many configurations due to their modular connection and create targets of different sizes and material composition. The targets' plastic coverage was also modified during the experiment to simulate different marine debris concentrations and evaluate the effect on the detection capability. For PLP2019 five target configurations were created:

i. The four 5 × 5 m targets were placed in line, forming a large 5 × 20 m target, with half covered with plastic bottles and half covered with plastic bags. The targets had 100% plastic coverage (date of configuration 18/4/2019).

ii. Each of the four 5 × 5 m targets was placed separately at a large distance from the rest. Two targets were covered with plastic bottles and the other two with plastic bags. Their coverage with plastic was 100%. Additionally, two elongated 1 × 10 m targets were constructed; one with plastic bottles and one mixed (with plastic bags and only the white plastic mesh) The two elongated targets were also 100% covered with plastics (date of configuration 3/5/2019).

iii. The four 5 × 5 m targets were placed in pairs and formed two large 5 × 10 m targets; one with plastic bottles and one with plastic bags—the two targets were 75% covered with plastics. On the same day, a smaller 2 × 5 m target was formed, containing 100% plastic bottles (date of configuration 18/5/2019).

iv. As in the previous case, the four 5 × 5 m targets were placed in pairs and formed two large 5 × 10 m targets, one with plastic bottles and one with plastic bags. This time the plastic coverage was reduced to 50%. Also, the smaller target (2 × 5 m) again had 100% coverage with plastic bottles (date of configuration 28/5/2019).

v. The four 5 × 5 m targets were placed together, forming one large 10 × 10 m target, half covered with plastic bottles and half with plastic bags. However, the plastic coverage of this large target was 25%. The smaller target (2 × 5 m) again had 100% coverage with plastic bottles. Additionally, a new 5 × 10 m target was created, which was fully covered with natural reeds (100% coverage) (date of configuration 7/6/2019).

2.2. Satellite Data

The PLP2019 was designed to run for the two months of May–June 2019. Since Sentinel-2 overpasses the Tsamakia Beach every five days, we planned for 13 measurements in total. Also, one measurement was made in April 2019, which served as a rehearsal for the following months. Unfortunately, due to clouds and bad weather, only five Sentinel-2 satellite images captured the test site in good weather conditions. On the remaining days either clouds prevented capture of the study area, or high wind-waves prevented the deployment of the targets. For all acquisition dates, Level-1C and Level-2 Sentinel-2 images were downloaded from the Copernicus Open Access Hub and archived.

The known geometric quality of the Sentinel-2 data is about a 10 m pixel [36]. For ensuring good positioning accuracy, a high-resolution orthophoto map created in PLP2018 (~0.03 m) was used as master image for improved geo-referencing of the Sentinel-2 images (~10 m). Uncertainties of the final positioning of Sentinel-2 were not thoroughly examined due to a lack of ground control points; however, we assume a value of 5 m (0.5 pixel of Sentinel-2).

The Level-1C data were atmospherically corrected using ACOLITE v. 20190326.0 (available at: http://odnature.naturalsciences.be/remsem/software-anddata/acolite/). ACOLITE is an open-source atmospheric correction and sun glint removal software, originally developed for aquatic scene processing of turbid waters [37]. Atmospheric correction with ACOLITE can be performed using two different correction methodologies; through an exponential extrapolation function (EXP) or a dark spectrum fitting (DSF) algorithm [38]. The DSF methodology is preferred over the EXP algorithm, since EXP assumes zero water-leaving reflectance in the SWIR bands and attributes any SWIR signal to Rayleigh and aerosol scattering, which can often be a false assumption. This is especially prevalent in the presence of sun glint, which is very common in nadir-viewing satellites such as the Sentinel-2, as well as in the case of adjacency effects. The DSF algorithm, which was used in this study, works by using two main assumptions to estimate the atmospheric path reflectance: i) the atmosphere is homogeneous over a certain extent; and ii) the scene contains pixels with zero reflectance, in at least one of the sensor bands [39]. By assuming zero reflectance in a reference band (usually a NIR or SWIR band), the glint signal can be estimated and computed for the other bands. ACOLITE estimates the glint signal in both SWIR bands (as in Harmel et al., 2018), with the band giving the lowest estimate for the glint signal being used to avoid negative reflectance values in the other Sentinel-2 SWIR band [40]. In addition to atmospheric correction, ACOLITE performs cloud masking using the 1600 nm band. A crude land mask was also applied using the NIR band at a reflectance threshold of 0.1. No ancillary data were used for the atmospheric correction processing. ACOLITE was used in this study instead of the default SEN2COR algorithm for S-2 products, due to results from Topouzelis et al. (2019) indicating that SEN2COR produces higher reflectance values for water constituents, which could interfere with floating plastics detection. However, since differences in the bottom-of-atmosphere reflectance can vary significantly between the two AC methodologies, further studies and intercomparison campaigns are needed in order to assess the suitability of different atmospheric correction algorithms using high-quality in situ measurements.

2.3. Unmanned Aerial System (UAS)

The use of UAS is crucial for calculating the actual position of the targets and is necessary for calculating the plastics coverage in the Sentinel-2 pixels. For each day that targets were deployed on the sea surface, a UAS captured their position. It is essential for the UAS capture to coincide with the satellite acquisition, due to the fact that the targets, despite being anchored, are not in a stable position.

Due to wind, waves, and currents they can move or tilt, up to some meters, which is problematic for precise positioning and therefore plastic coverage calculation on Sentinel-2 pixels.

During PLP2019, effort was made for the UAS images to be captured simultaneously with Sentinel-2 acquisition. However, this was not achieved on all the experimental days due to several technical problems. In general, the UAS images had a time difference with the Sentinel-2 images of over 30 minutes (Table 1). We believe that this difference does not seriously affect the position of the targets and any displacement of targets is not significant for the final plastic coverage calculation.

Table 1. Time difference between Sentinel-2 acquisition and UAS acquisition.

Date (yyyymmdd)	Approx. Sentinel-2 Acquisition (Local Time)	UAS Acquisition (Local Time)	Time Difference
20190418	12:00	13:46	1 hr and 46 minutes
20190503	12:00	11:34	26 minutes
20190518	12:00	11:27	33 minutes
20190528	12:00	12:51	51 minutes
20190607	12:00	11:30	30 minutes

In PLP2019 a DJI Phantom 4 drone was used, equipped with a 12.4 M pixel camera, capturing 4000×3000 pixel images. This UAS has a GLONASS satellite positioning system, which provides a vertical accuracy range of ±1.5 m. The UAS flight height was around 100 m above the sea surface, and the produced spatial resolution of the images was 3–4 cm. The Phantom 4 was selected in preference to larger drones with DGPS capabilities due to its small size, extensive flight time and flexibility in the field. Also, from PLP2018, we understood that no orthophoto maps of the larger area were needed. Only the target area needed to be captured and positioned accurately in space. Accurate positioning is achieved by georeferencing the UAS images with a high-resolution orthophoto map created in PLP2018. For all UAS images, known ground control points (GCPs) on the beach and on coastal habitats are used. The UAS georeferencing was very successful, with a mean positioning error of less than 15 cm. However, the need for GCPs located on the beach forced the drone team to capture images with an oblique view in most cases. This distortion was later evident in the calculation of the actual size of the targets. To ensure the actual positioning of the targets, GPS signals of the targets were overlaid on the georeferenced images. The mean positioning error between the GPS and the georeferenced images was less than 0.5 m, which is assumed satisfactory considering the vertical accuracy of GPSs.

The data used in this study, i.e., the Sentinel-2 L1C granules catalogue, Sentinel-2 L2 subsets (after pre-processing with ACOLITE) and the percentage plastic presence for each Sentinel-2 pixel, can be downloaded from the University of the Aegean's Marine Remote Sensing Group web page http://mrsg.aegean.gr and from ZENODO database (https://doi.org/10.5281/zenodo.3752719). Annex A contains the description of the available dataset.

2.4. Methodology-Detection Perspective

The methodological framework for the detection of floating marine plastics is in its infancy. Several parameters influence the detection—i.e., atmospheric correction, white caps, sun glint, clouds, cloud shadows, waves, and plastic concentration—and we are still far from being able to rely on an accurate detection algorithm. Here, we develop a methodology to calculate the presence of plastic in the Sentinel-2 pixel with the use of UAS images (Figure 2). Then we examine the spectral behavior of the pixel according to the plastic coverage, and we use spectral unmixing and matched filtering techniques to ensure the connection of lab spectral signatures with the natural environment. As a third step, we examine the use of the developed methodology as a proxy for litter detection in larger areas.

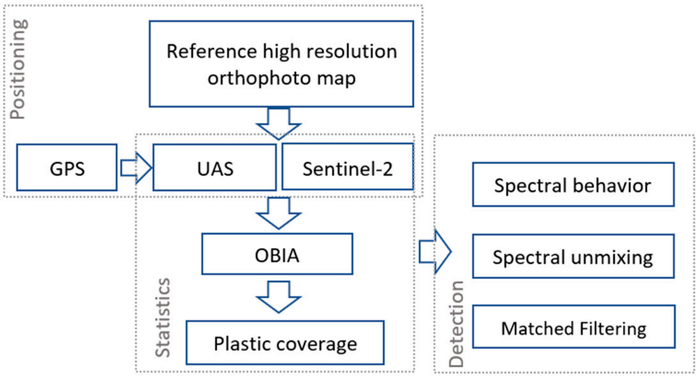

Figure 2. Flow diagram on the developed methodology on percentage plastic coverage calculation using UAS and Sentinel-2 datasets and on detection techniques.

2.4.1. Plastic Coverage and Spectral Behavior on Sentinel-2 Images

Sentinel-2 images were georeferenced with the use of a high-resolution orthophoto map. Although no sensitivity analysis was performed on the positional accuracy, in all cases except one (the 20190503 image), the percentage differences in the plastic coverage before and after the georeferencing was negligible, i.e., 0–2%. This finding can lead us to the assumption that, in most cases, the Sentinel-2 geometric accuracy is high enough, and no further georeferencing is necessary for the plastic detection.

For each Sentinel-2 pixel containing plastic, we calculate the percentage plastic coverage, and we extract the spectral data. The pixel coverage was determined through object-based image analysis. Initially, a region of interest (ROI) was determined in each Sentinel-2 image in order to isolate the study area. Then the ROI of the Sentinel-2 and UAS data was inserted in the eCognition Developer 9.5.1 software and, through a multiresolution segmentation (using scale: 140, shape: 0.1, compactness: 0.9) and manual classification, targets were classified in the UAS layer. Each plastic target was coded with a capital letter (e.g., A, B, C) and each Sentinel-2 pixel was numbered accordingly (e.g., A1, A2, . . . , Ax). Then, the percentage of plastic coverage was extracted for each pixel of Sentinel-2 based on its relation to UAS sub-objects (Figure 3). The spectral behavior of the plastic targets was further investigated by extracting and analyzing the values of the relevant pixels in comparison with the clear surrounding waters.

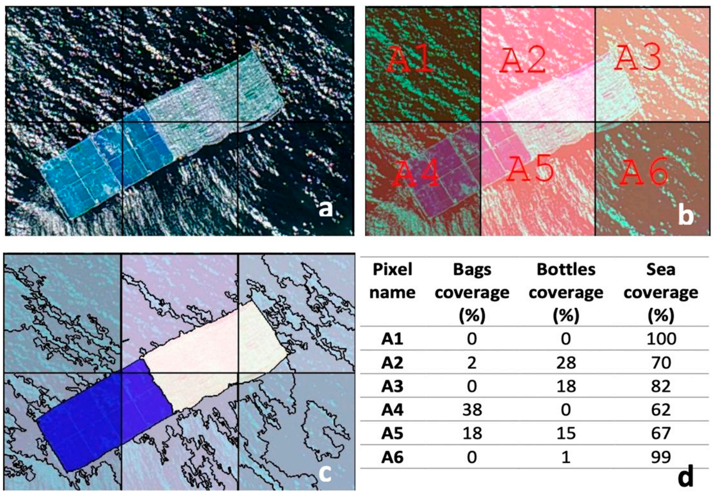

Pixel name	Bags coverage (%)	Bottles coverage (%)	Sea coverage (%)
A1	0	0	100
A2	2	28	70
A3	0	18	82
A4	38	0	62
A5	18	15	67
A6	0	1	99

Figure 3. Example of the plastic coverage calculation using UAS data on a Sentinel-2 image from 18th April 2019. (**a**) UAS image overlaid with Sentinel-2 pixel grid; (**b**) Sentinel-2 pixels names with UAS data transparency; (**c**) object based classification of plastic bags (blue), plastic bottles (white), and sea (cyan); (**d**) percentage calculation of the plastic presence in each Sentinel-2 pixel.

2.4.2. Spectral Unmixing and Matched Filtering

Linear spectral unmixing is routinely used with hyperspectral data, in order to decompose the spectral signature of a mixed pixel into a set of endmembers and their corresponding abundances. The theoretical basis behind the approach is that given a mixed pixel comprising different materials/endmembers with different spectral signatures, the spectral signature of the pixel will be a mix of different signatures described by a linear relationship, based on the abundance fractions of the materials. If the individual spectral signatures are known, the pixel abundance fractions can be calculated. Although spectral unmixing generally requires a large number of bands, and is therefore used mainly with hyperspectral data, a smaller number of bands can also be used, provided that the available number of bands is larger than the number of pixel endmembers. Equation (1) shows the simple linear mathematical expression that describes the theory behind spectral unmixing given two-pixel endmembers; where R_{mix} is the mixed pixel reflectance for wavelength λ, f_p, and f_w are the plastic target and seawater endmember abundance fractions respectively, and R_p and R_w are the reflectances for the plastic target and seawater endmembers for wavelength λ, respectively.

$$R_{mix}(\lambda) = f_p \times R_p(\lambda) + f_w \times R_w(\lambda) \tag{1}$$

In this study, we used an inverse spectral unmixing approach (Equation (2)), where the pixel abundance fractions are the known variables, and the target spectral signatures are the unknown variables. Since no pure pixels that are solely composed of floating marine plastics are present in any of the images acquired during PLP2018 and 2019, it was not possible to directly acquire a spectral signature for the marine plastic targets. Through the inverse spectral unmixing process, we can estimate the spectral response of the marine plastic targets, without the need for a pure pixel.

$$R_p(\lambda) = \frac{R_{mix}(\lambda) - f_W \times R_W(\lambda)}{f_p} \tag{2}$$

For the inverse spectral unmixing process, we used the pixel percentage coverages that were calculated for PLP2018 [10]. The abundance fractions for each pixel and the spectral signature for seawater are inserted in the rearranged Equation (2), which produces the spectral response of the target materials for each wavelength that is used. The small size of the targets indicates that only the four 10 m bands of Sentinel-2 can be used in the spectral unmixing process, since the 20 m band pixels are not sufficiently covered by the target materials to produce a proportionately relevant response. In this approach, only the PET target pixels were used for the calculation of the spectral signature, because they gave the highest response compared with the plastic bag and net targets. In addition, no spectral signature for blue LDPE bags could be found in the published literature. For the seawater signature, we used both the signature from the surrounding waters and the spectral signature for coastal waters from the USGS spectral library v.7 [41]. With both signatures yielding similar results, the USGS signature for coastal waters was used for consistency in all calculations.

Matched filtering (MF) is a process commonly used in a variety of applications in order to detect the presence of a known signal or signature, in a mixed signal of unknown components and/or noise [42,43]. In image processing, matched filtering can be used to calculate the abundance of a known endmember by essentially performing a partial unmixing, without the need to define all the endmembers present in a pixel. Much like linear spectral unmixing, MF uses a linear model for subpixel analysis, but removes the requirement to determine all the endmembers by maximizing the response of a known endmember and suppressing the signal of the unknown background. ENVI v5.5.2 was used to perform the spectral unmixing and matched filtering processing.

3. Results and Discussion

3.1. Plastic Coverage Calculation

In Figure 3, an example of the percentage plastic coverage of Sentinel-2 pixels is given for the 20190418 image. The UAS image is used as a base map and the Sentinel-2 pixels are overlaid as a grid. For each pixel with plastic, a dedicated name is visible. Next, the UAS image is segmented in eCognition Development 9.5.1 software with a multiresolution segmentation algorithm and the segments are manually classified into three categories: sea, bottles, and bags. The image segmentation result in relation to the Sentinel-2 grid led to the percentage calculation of the plastic coverage for each pixel. In Figure 3, the A1 and A6 pixels do not contain plastic, the A4 pixel is 38% covered with plastic bags and 62% is sea, the A3 pixel contains 18% plastic bottles and 82% sea, and the A5 is a mixed Sentinel-2 pixel with 18% bags, 15% bottles, and 57% sea.

3.2. Spectral Behavior of the Plastic Targets

Most target pixels from all acquisition dates have a similar spectral response, with differentiation mostly in the intensity but not the shape of the signal. However, the plastic bags targets were significantly wetted or even slightly submerged when deployed at sea. Wet materials produce a significantly lower response than dry materials [24] and in addition, with the blue color of the bags, the 5 × 5 m plastic bags targets did not produce a spectral response that was discernible from the water background and therefore were not further examined. All the primary target pixels—those with the highest response and hence the greatest plastic abundance fractions—show significant spectral similarities, with spectral angles of less than 10° (varying between 3° and 9°). Figure 4 presents an example of spectral signatures of pixels containing part of the plastic targets. The four signatures shown correspond to the four pixels that were detected through the matched filtering processing. The reflectance peaks were in the NIR and visible range, with a downward slope from the blue 443 nm to the red 665 nm bands. This is in contrast with the fact that most non-colored plastics have an almost flat spectral response across the visible range of the electromagnetic spectrum, with distinct and characteristic absorption bands in the NIR and SWIR range [24]. This inconsistency can be attributed to several factors.

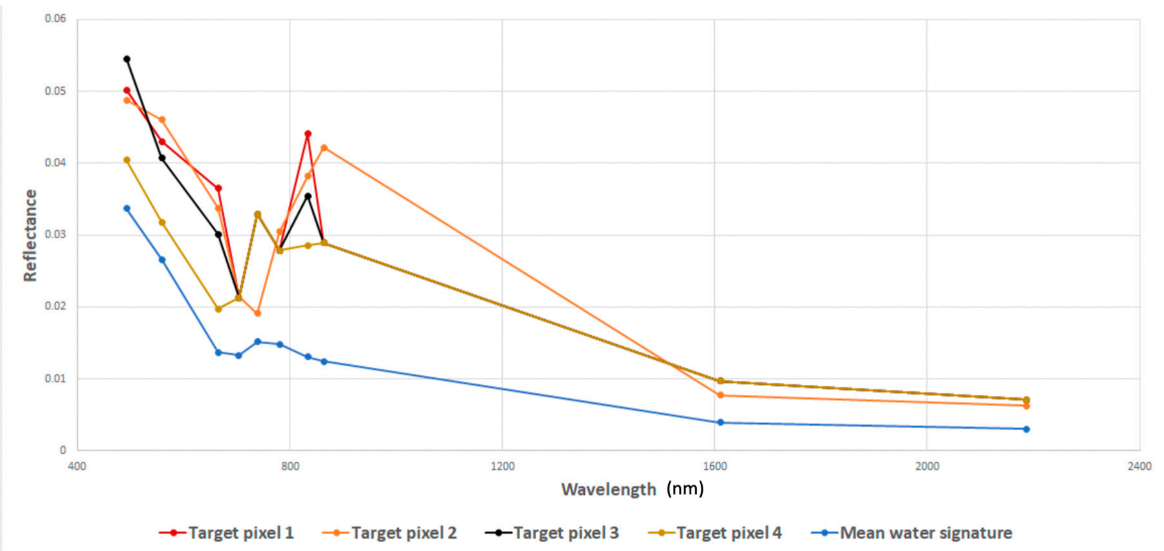

Figure 4. Spectral signature of the four detected target pixels on the 20190418 experimental date. The four Sentinel-2 pixels contain different percentage plastic coverage and are illustrated in the first row of Figure 5.

First and foremost, the Sentinel-2 spatial resolution of the RGB and NIR bands is higher (at 10 m) than the other bands (20 m and 60 m resolution). Hence, the targets' size and position in the image matrix play a significant role in the spectral response that is acquired, as the higher spatial resolution of the RGB and NIR bands makes them more sensitive to smaller targets. In theory, if the artificial targets were of a large enough area to cover a 20×20 m pixel, the spectral response of the PET targets would be expected to be almost flat, with a slight upward slope from blue to red wavelengths and dips in the SWIR range due to the absorption features of the material [41]. Also, both seawater and bottom reflectance contribute to some degree to the spectral response of the target pixels. The weak seawater signal generally peaks at the blue range of the spectrum, with coastal waters presenting some variation due to increased optically active constituents (e.g., chlorophyll, suspended matter, etc.). Although effort was made for the targets to be placed on top of seagrass meadows for simulating a dark substrate, bottom reflectance is still present in the overall signal, as the water column between the targets and the seafloor was not optically deep. Both these factors contribute to the target pixels' signal, altering the response in the visible range of the spectrum.

Other parameters have also been identified as having an impact on the spectral response of the target pixels or the detection capabilities. Sun glint, a significant implication regarding marine remote sensing applications, is a major confining factor regarding marine plastic detection. The nadir-viewing geometry of the Sentinel-2 satellite makes it especially susceptible to sun glint [40]. In combination with the acquisition time over the Mediterranean (close to solar noon) and the acquisition dates (spring and summer), all of the acquired images are to some degree contaminated with sun glint. Sharp glint cannot be corrected for, and pixels dominated by a high glint signal need to be masked out from further analysis using simple geometric calculations based on sun and viewing angles and/or brightness thresholds. Weak glint, on the other hand, can be corrected for, with most deglinting algorithms using the NIR or SWIR bands to perform the correction [40,44]. The sun glint removal algorithms are based on the assumption that seawater absorbs all infrared radiation; hence any water-leaving reflectance in the NIR and SWIR regions of the spectrum can be solely attributed to sun glint. Much like a dark spectrum fitting algorithm for atmospheric correction, the deglinting algorithms use the lowest NIR or SWIR value as reference and correct all pixels above that value, as they are identified as pixels affected by glint. This process works fine in applications where the NIR and SWIR response can indeed be solely attributed to sun glint. However, floating marine plastics produce a significant response in the NIR and SWIR regions of the spectrum, which can be highly important in terms of detection capabilities. Hence, correcting for glint using the NIR or SWIR bands as reference would inevitably also alter the signal of any pixel that contains marine plastics, even if that pixel is not affected by sun glint.

Besides sun glint, a second affecting factor inherent in marine remote sensing applications is the introduction of bidirectional reflectance effects in Sentinel-2 data. This effect is due to the configured operation of the sensor detector, which is more evident over the ocean due to water's inherent optical properties [45]. Kremezi and Karathanassi showed that the bidirectional reflectance distribution function (BRDF) effects are more prevalent for the detectors further away from the nadir-viewing sixth and seventh detectors. In the present study, the pixels of interest were on the interface of the fourth and fifth detector footprints, which are shown to have minimal BRDF effects. As such, it was deemed that there is no need to perform a BRDF correction. However, the BRDF effects, while minimal, could significantly impact the spectral response of the targets and hence the detection capabilities and results. Consequently, it is considered necessary to further evaluate the BRDF effects over water bodies in Sentinel-2 images, specifically for marine plastics detection.

In addition, since marine plastics concentrations produce a weak signal, a high signal-to-noise ratio (SNR) is considered necessary for the accurate detection of floating marine plastics [11]. Thus, it is essential to assess the detection capabilities of the Sentinel-2 satellite based on each band's SNR, in order to evaluate the minimum concentrations that can be accurately detected without a large number of false positives. This assessment is also essential in order to determine an appropriate SNR for further missions specifically targeted for marine plastics detection.

3.3. Spectral Unmixing and Matched Filtering

Initially, the spectral signature for PET from the USGS spectral library v.7 [41] was used as the primary endmember to perform a linear spectral unmixing algorithm on the PLP2018 image, i.e., the 20180607 image. The results showed that using the USGS PET signature significantly underestimated the abundance fraction of the PET target pixels in the 20180607 image, when compared to those in Topouzelis et al. [10]. For this reason, we performed a reverse spectral unmixing process using the four pixels that contained PET concentrations in the 20180607 image, as described in 2.4.2. In theory, we would expect that all four pixels would yield the same response for the four 10 m bands, in essence producing a single signature characteristic of the target material. However, the results varied significantly in the three RGB bands, but were very similar for the NIR band. This observation is attributed to two main factors. Firstly, although efforts were made to set the targets on top of a dark substrate, the water column between the targets and the seafloor was not optically deep. As a result, bottom reflection affects the overall pixel signal, and therefore the derived spectral signatures are not consistent in the visible bands. Secondly, since water absorbs almost the entirety of infrared radiation in the NIR band, the NIR response can be solely attributed to the target materials (provided that no significant glint is present in the area of interest, which could affect the NIR response). The above statement is supported by the fact that the reverse spectral unmixing calculations produce very similar values in the NIR band for all pixels affected by the PET target. To produce an applicable signature for further processing, the USGS signature for PET was modified by reducing the intensity of the signal so that the NIR reflectance value matches the one that was calculated through the reverse spectral unmixing methodology. The produced signature was then used to perform a linear spectral unmixing calculation in order to verify the applicability of the PET signature using the PLP2018 data. Although the abundance fractions were underestimated for some pixels, the spectral unmixing results were very similar to those obtained through the UAS orthophoto and hence the spectral signature was deemed suitable to be used for the matched filtering processing.

The matched filtering processing was applied to all six images acquired through the 2018 and 2019 PLPs, to assess the capability to use this methodology for the purposes of detecting and quantifying floating marine plastics. Figure 5 presents the results of the matched filtering methodology applied to subscene cutouts of the six Sentinel-2 products. The matched filtering methodology underestimates the abundance fractions of the mixed pixels in the 20180607 image (from 24% to 66%); however, the overall results match the degree of coverage (i.e., pixels with higher plastic coverages are correctly identified as having higher coverage than pixels with lower coverages). Although the matched filtering methodology has been applied using only the PET signature, pixels containing part of the mesh or the bags targets from PLP2018 can also be identified, with lower abundance fractions than those calculated through the UAS images. Therefore, a bulk signature could potentially be used for the detection of a variety of floating marine plastics. The results indicate that the matched filtering methodology can be successfully applied (using the modified USGS signature for PET) for detecting pixels with an abundance fraction of PET of at least as low as 25%. For instance, in the 20190503 image a single pixel can be detected, which corresponds at most to a 25 m^2 plastic target on a 100 m^2 pixel, assuming the target is captured in a single pixel. The second PET target however is not detected, most likely since the 5×5 m target is positioned in such a way that the plastic concentration is distributed over several pixels.

This observation is supported by the 20190518 results as well, where two pixels corresponding to the targets can be identified. The percentage coverage of the targets for that date was 75%, and hence the maximum abundance fraction for a single pixel can be 37.5%. Since two pixels are identified, this translates to less than 20%-pixel coverage for PET. However, the mesh below the bottles affects the signature, and hence the abundance fraction of PET is slightly overestimated. The bottom part of the 20190518 subscene is contaminated with low clouds and/or a high aerosol content that have not been corrected for with the atmospheric correction processing. Hence, a procedure to remove pixels that are profoundly affected by atmospheric parameters is needed.

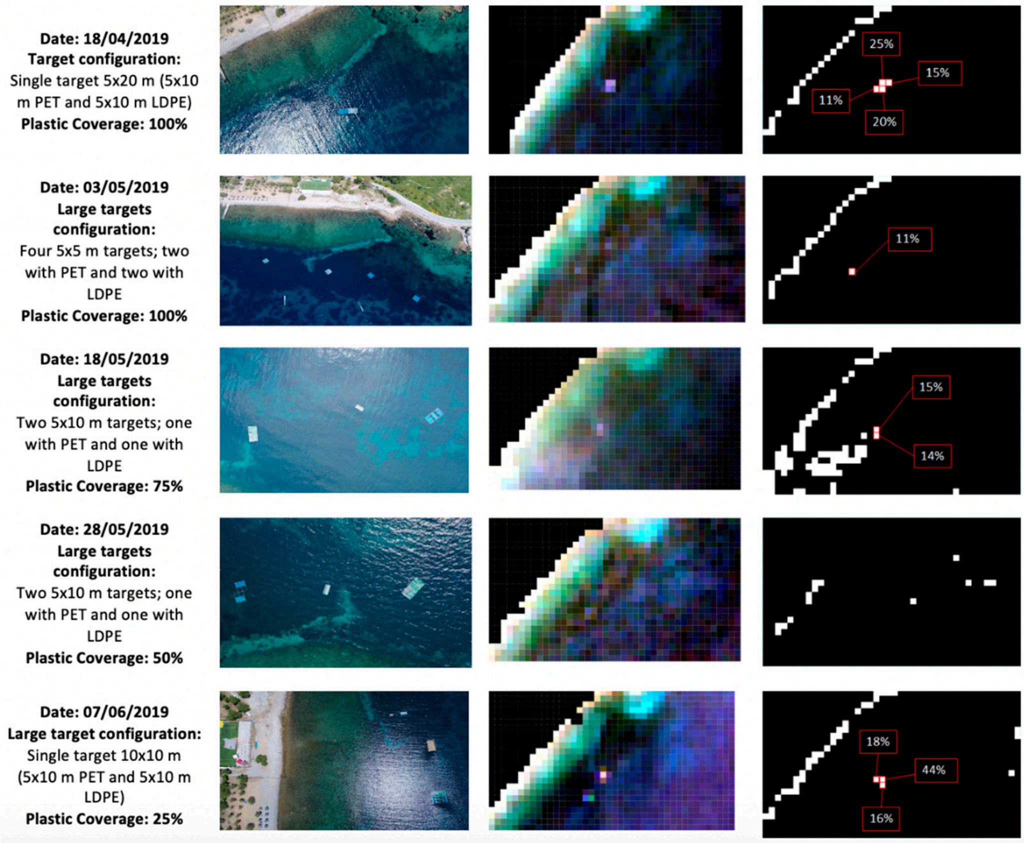

Figure 5. Target description and results. From left to right: description of the artificial targets configuration, UAS reference images, Sentinel-2 sub scenes after ACOLITE pre-processing, and results of the matched filtering detection.

Weak wave glint can affect the matched filtering results, overestimating the presence of PET in a pixel, but this effect does not seem to produce abundance fractions that are higher than 10–15%. Therefore, weak sun glint can be mitigated by using an appropriate threshold based on the degree of glint contamination. More intense glint, as in the case of the 20190528 image, has a significant impact on the capability to correctly estimate the PET abundance fraction, because the glint signal markedly alters the water-leaving reflectance. The glint correction methodology applied through ACOLITE did not sufficiently mitigate the effect of sun glint contamination in the area of interest, and the target pixels were not detectable through the matched filtering processing. It is unclear, however, if a larger 10×10 m target would be detectable regardless of glint contamination. In the case of the 20190607 image, although the PET and bags target is 10×10 m, the fact that the coverage of the target has been reduced to 25% prevents the detection of the target pixels, given the 10% threshold. The pixels that are marked as containing PET abundance fractions at the right end of the image correspond to pixels that are affected by weak wave glint and produce an abundance fraction slightly higher than the set threshold of 10%. The reeds target pixels are marked as if they contain a large abundance fraction of PET (higher than 15%). This result is consistent with the higher signal that these targets produced, and indicates that it is not possible to distinguish between plastic and natural marine debris using the matched filtering methodology alone, at least not without using a second endmember for natural debris. The presence of plastic bags in a mixed pixel is interpreted as a lower PET concentration from the matched filtering processing. This observation indicates that a bulk floating marine plastics signature can be used to assess the presence of a variety of marine plastic types.

When the matched filtering methodology is applied to a larger coastal area, all the pixels close to the coastline are identified as containing PET abundance fractions due to the bottom reflectance influence. This observation indicates that besides the use of a land mask, the detection methodology must remove the pixels that are most affected by bottom reflectance. This removal could be achieved by using a geographically based land mask that is buffered to mask out all pixels that are affected by bottom reflectance. Figure 6 shows an example of the matched filtering results when the methodology is applied to a complete Sentinel-2granule product. For the 20190418 image, the results show that four pixels containing floating marine plastics can be successfully identified. This image is not significantly affected by wave glint, and the effects of bottom reflectance lead to the entire coastline being marked as containing floating marine plastics abundance fractions. Other false positives include mainly vessels, exhaust fumes, cloud shadows and outlines.

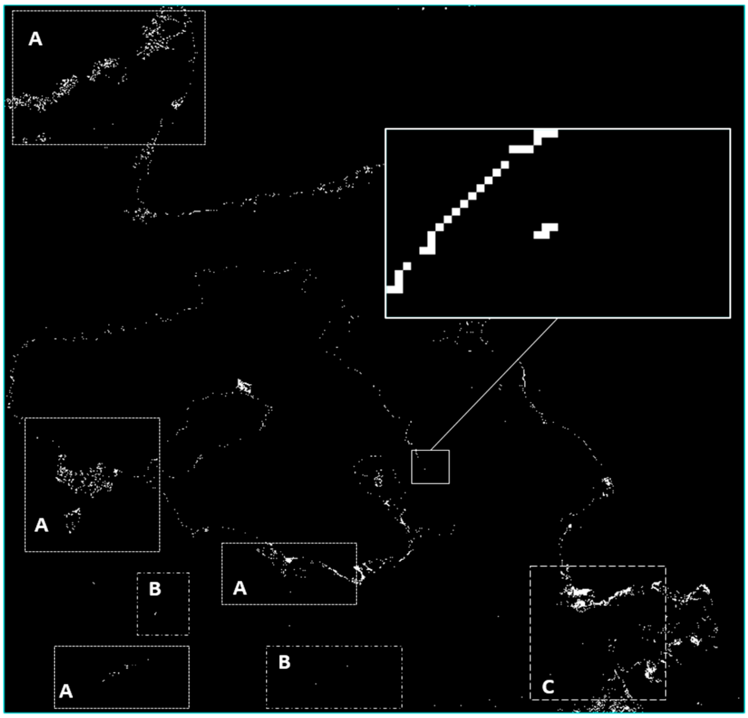

Figure 6. Example of the matched filtering results in a complete Sentinel-2 product for the 18 April 2019 image. A cutout of the plastic targets pixels that are detected is shown in the middle right part of the image in the bold white square. Areas indicated with 'A' represent commission errors due to cloud outlines and shadows; 'B' false detection of vessels, wakes and exhaust fumes and 'C' false detection of pixels contaminated with intense sun glint. Almost the entire coastline is falsely classified due to bottom reflectance and/or adjacency effects.

All the above-identified factors—namely, sun glint, clouds, cloud outlines, cloud shadows, bottom reflection, vessels, and exhaust plumes—are factors that can significantly affect the matched filtering results. Hence, these effects will need to be mitigated for the methodology to be successfully applied as a floating marine plastics detection process. However, the matched filtering methodology can be applied in tandem with separate detection processes using different methodologies to provide floating marine plastics quantification capabilities.

4. Conclusions and Outlook

Atmospheric correction and sun glint removal play a vital role in the plastic return signal, and therefore in the detection efficiency. Although ACOLITE is used in this paper for both atmospheric correction and sun glint removal, further studies need to evaluate the suitability of atmospheric correction methodologies specifically for floating marine plastics detection applications. Hence, in situ measurements using field spectrometry, which can be performed during campaigns such as the PLPs, are crucial, as they are a prerequisite for the assessment, calibration, and validation of atmospheric correction methodologies such as SEN2COR, C2RCC, and iCOR. In addition, glint correction is an essential pre-processing step when dealing with aquatic scenes acquired with nadir-viewing sensors, and this includes floating marine plastics detection applications. However, present glint correction algorithms that use the SWIR or NIR bands inevitably interfere with the plastics signal, compromising the detection of floating marine litter. Due to the non-zero signal of plastics in the NIR and SWIR part of the spectrum, pixels that are not affected by glint but contain floating plastics would be corrected for glint, reducing the signal intensity. In this context, the development of a glint correction methodology that does not interfere with the presence of floating plastics in a pixel would be a major improvement. Alternatively, a detection methodology that is not affected by the presence of glint would render the deglinting process redundant.

The precise location of the targets and their observations (i.e., UAS and Sentinel-2 images) is crucial for quantitative assessment. Targets should contain two GPS with the highest available positioning accuracy so as to understand their orientation. UAS aerial images should be acquired simultaneously with satellite acquisition with the smallest oblique distortion, in order to avoid complications during image georeferencing. This synchronization is vital for mutual comparison purposes and for ensuring the actual pixel coverage of Sentinel-2 images. Similar to the plastic targets, UAS should be equipped with a DGPS positioning capability to ensure the positioning accuracy of the aerial images. Additionally, ground control points should be used in the study area to cross-validate the positioning of both the targets and the aerial images. Sentinel-2 images have a good georeferencing with circa a single 10 m pixel geometric position; however, large control points in the coastal area can further improve their positioning accuracy.

Given proper weather conditions (i.e., relatively calm seas, low glint contamination, minimal cloud cover), the methodological approach described here can be used to successfully detect pixels with a PET abundance fraction of at least as low as 25%. The results show that, when using the PET signature, the methodology overestimates the abundance fraction of pixels containing part of the reeds target and underestimates the fractions of pixels contaminated with plastic bags. This inconsistency suggests that the methodology may not be suitable for differentiating between different types of floating debris, at least not without using more bands and endmembers to perform the analysis. However, the detection of all types of targets using the PET signature suggests that a bulk signature can be used for the detection and quantification of floating marine debris. Hence, the production of a characteristic floating plastic spectral signature is essential for further development. Towards this goal, future experimental campaigns should focus on the acquisition of reference images with characteristic marine plastics for producing a relevant bulk signature.

Another prerequisite is the construction of artificial targets with an effective area large enough to guarantee at least a full coverage of a 10 × 10 m Sentinel-2 pixel, regardless of target orientation. A full pixel coverage is essential to guarantee a meaningful reference signature which can be used as-is, without the need to perform inverse spectral unmixing calculations. Additionally, a target size that would guarantee full coverage of a 20 × 20 m pixel would also allow for proper analysis of the SWIR and red edge target signals. These wavelengths are significant for detection capabilities, as well as the assessment of atmospheric correction and glint correction methodologies.

Besides the target dimensions and materials, an essential requirement is a high number of data acquisitions. Future campaigns should work towards the deployment of semi-permanent targets that allow for continuous data acquisition without the need for target re-deployment, in order to reduce the logistical needs and increase the data acquisition capabilities. Field campaigns such as the PLPs can provide the necessary ground-truth data that are an essential requirement for the calibration and validation of floating marine debris detection methodologies, as well as the assessment of future mission requirements such as sensor SNRs and radiometric resolutions. While the target sizes, composition, deployment site, and conditions can vary, it is of vital importance that similar campaigns are developed and executed all over the globe.

Further calibration and validation studies such as the PLPs, along with the evolution of the proposed and other detection methodologies to an operational stage, are a necessary step for the development of a global marine debris monitoring system. Such a monitoring system would represent a significant tool for the calculation of a floating plastic litter mass budget, alongside more traditional methods such as surface trawling and modeling. Perhaps more importantly, an automated global- and local-scale monitoring system would enable specialized targeted marine debris removal campaigns, allowing for timelier and less costly and resource intensive approaches. A timely removal of plastic marine debris would prevent sinking of otherwise buoyant litter due to biofouling, as well as degradation of macroplastic items into microplastics, after which their removal is very difficult and the impact to the environment much graver.

Author Contributions: Conceptualization: K.T.; Methodology: K.T. and D.P.; Validation: K.T., D.P., A.K., and A.P.; Formal analysis: K.T., D.P., and A.K.; Investigation: K.T., D.P., and A.K.; Resources: K.T., and M.A.B.; Data curation: K.T., and A.K.; Writing—original draft preparation: all authors. All authors have read and agreed to the published version of the manuscript.

Funding: This research was partially funded by European Space Agency (ESA)-EO Science for Society permanently open call. Project: "EO tracking of marine debris in the Mediterranean Sea from public satellites".

Acknowledgments: We would like to thank Marine Remote Sensing Group member Michaela Doukari for helping in the orthophoto creation and data georeferencing. Target construction was completed by undergraduate and postgraduate students in the Department of Marine Studies at the University of the Aegean. We wish to acknowledge the Municipal Port Fund of Lesvos, Municipality of Lesvos Island, and Mytilene Sailing Club for their support during the experiment.

Conflicts of Interest: The authors declare no conflict of interest.

Appendix A. Description of Shareable PLP2019 Data Set

The data used for the present study can be downloaded from the University of the Aegean's Marine Remote Sensing Group web page https://mrsg.aegean.gr/ and from ZENODO database (https://doi.org/10.5281/zenodo.3752719). The dataset contains:

i. Sentinel-2 L1C granules catalogue in a word document named: "PLP2019 Sentinel-2 Image Catalogue",
ii. Sentinel-2 L2 subsets after pre-processing with ACOLITE i.e., after atmospheric correction, sun glint removal and land making. Data are given in netCDF format (.nc) in a folder named "S2_satellite_images_nc",
iii. UAS images with the plastic targets for each date. UAS images are organised in the folder named "UAV_photos",
iv. Point vectors with percentage plastic presence for each Sentinel-2 pixel in the folder "Vector_Points". Point vectors are given in ERSI vector and are organised by the acquisition date. Also, for each date an Excel file is provided to locate and describe the name of the actual pixel.

References

1. Ryan, P.G. A Brief History of Marine Litter Research. In *Marine Anthropogenic Litter*; Springer International Publishing: Cham, Switzerland, 2015; pp. 1–25.
2. Portman, M.E.; Brennan, R.E. Marine litter from beach-based sources: Case study of an Eastern Mediterranean coastal town. *Waste Manag.* **2017**, *69*, 535–544. [CrossRef]
3. Suaria, G.; Aliani, S. Floating debris in the Mediterranean Sea. *Mar. Pollut. Bull.* **2014**, *86*, 494–504. [CrossRef]
4. Mansui, J.; Darmon, G.; Ballerini, T.; van Canneyt, O.; Ourmieres, Y.; Miaud, C. Predicting marine litter accumulation patterns in the Mediterranean basin: Spatio-temporal variability and comparison with empirical data. *Prog. Oceanogr.* **2020**, *182*, 102268. [CrossRef]
5. Meyerjürgens, J.; Badewien, T.H.; Garaba, S.P.; Wolff, J.-O.; Zielinski, O. A State-of-the-Art Compact Surface Drifter Reveals Pathways of Floating Marine Litter in the German Bight. *Front. Mar. Sci.* **2019**, *6*, 1–15. [CrossRef]

6. Van Sebille, E.; Aliani, S.; Law, K.L.; Maximenko, N.; Alsina, J.M.; Bagaev, A.; Bergmann, M.; Chapron, B.; Chubarenko, I.; Cózar, A.; et al. The physical oceanography of the transport of floating marine debris. *Environ. Res. Lett.* **2020**, *15*, 023003. [CrossRef]
7. Liubartseva, S.; Coppini, G.; Lecci, R.; Clementi, E. Tracking plastics in the Mediterranean: 2D Lagrangian model. *Mar. Pollut. Bull.* **2018**, *129*, 151–162. [CrossRef]
8. Politikos, D.V.; Ioakeimidis, C.; Papatheodorou, G.; Tsiaras, K. Modeling the Fate and Distribution of Floating Litter Particles in the Aegean Sea (E. Mediterranean). *Front. Mar. Sci.* **2017**, *4*, 1–18. [CrossRef]
9. Prevenios, M.; Zeri, C.; Tsangaris, C.; Liubartseva, S.; Fakiris, E.; Papatheodorou, G. Beach litter dynamics on Mediterranean coasts: Distinguishing sources and pathways. *Mar. Pollut. Bull.* **2017**, *129*, 448–457. [CrossRef]
10. Topouzelis, K.; Papakonstantinou, A.; Garaba, S.P. Detection of floating plastics from satellite and unmanned aerial systems (Plastic Litter Project 2018). *Int. J. Appl. Earth Obs Geoinf.* **2019**, *79*, 175–183. [CrossRef]
11. Martínez-Vicente, V.; Clark, J.R.; Corradi, P.; Aliani, S.; Arias, M.; Bochow, M.; Bonnery, G.; Cole, M.; Cózar, A.; Donnelly, R.; et al. Measuring Marine Plastic Debris from Space: Initial Assessment of Observation Requirements. *Remote Sens. Environ.* **2019**, *11*, 2443. [CrossRef]
12. Biermann, L.; Vincente, V.M.; Sailley, S.; Mata, A.; Steele, C. Towards a method for detecting macroplastics by satellite: Examining Sentinel-2 earth observation data for floating debris in the coastal zone. *Geophys. Res. Abstr.* **2019**, *21*, 2019–17469.
13. Maximenko, N.; Corradi, P.; Law, K.L.; Van Sebille, E.; Garaba, S.P.; Lampitt, R.S.; Galgani, F.; Martinez-Vicente, V.; Goddijn-Murphy, L.; Veiga, J.M.; et al. Toward the Integrated Marine Debris Observing System. *Front. Mar. Sci.* **2019**, *6*, 447. [CrossRef]
14. GESAMP. *Guidelines for the Monitoring and Assessment of Plastic Litter in the Ocean*; United Nations Environment Programme: Nairobi, Kenya, 2019; Volume 99.
15. Garello, R.; Plag, H.-P.; Shapiro, A.; Martinez, S.; Pearlman, J.; Pendleton, L. Technologies for Observing and Monitoring Plastics in the Oceans. In Proceedings of the OCEANS 2019-Marseille, Marseille, France, 17–20 June 2019; pp. 1–6.
16. JRC. *Marine Litter Technical Recommendations for the Implementation of MSFD Requirements*; Publications Office of the European Union: Luxemburg, 2011.
17. Maximenko, N.; Centurioni, L.; Chao, Y.; Dohan, K.; Galgani, F.; Hardesty, B.D.; Law, K.L.; Moller, D.; van Sebille, E.; Wilcox, C. Remote sensing of marine debris. In *White Paper for the Earth Science and Applications from Space Decadal Survey: Space Studies Board*; USA National Academies of Science, Engineering and Medicine: Washington, DC, USA, 2016.
18. Hanke, G.; Werber, S.; Galgani, F.; Mira Veiga, J.; Ferreira, M. *Guidance on Monitoring of Marine Litter in European Seas*; Publications Office of the European Union: Luxemburg, 2013.
19. Goddijn-Murphy, L.; Williamson, B. On Thermal Infrared Remote Sensing of Plastic Pollution in Natural Waters. *Remote Sens.* **2019**, *11*, 2159. [CrossRef]
20. Goddijn-Murphy, L.; Dufaur, J. Proof of concept for a model of light reflectance of plastics floating on natural waters. *Mar. Pollut. Bull.* **2018**, *135*, 1145–1157. [CrossRef]
21. Garaba, S.P.; Dierssen, H.M. Hyperspectral ultraviolet to shortwave infrared characteristics of marine-harvested, washed ashore and virgin plastics. *Earth Syst. Sci. Data Discuss.* **2019**, 77–86. [CrossRef]
22. Goddijn-Murphy, L.; Peters, S.; van Sebille, E.; James, N.A.; Gibb, S. Concept for a hyperspectral remote sensing algorithm for floating marine macro plastics. *Mar. Pollut. Bull.* **2018**, *126*, 255–262. [CrossRef]
23. Garaba, S.P.; Aitken, J.; Slat, B.; Dierssen, H.M.; Lebreton, L.; Zielinski, O.; Reisser, J. Sensing Ocean Plastics with an Airborne Hyperspectral Shortwave Infrared Imager. *Environ. Sci. Technol.* **2018**, *52*, 11699–11707. [CrossRef]
24. Garaba, S.P.; Dierssen, H.M. An airborne remote sensing case study of synthetic hydrocarbon detection using short wave infrared absorption features identified from marine-harvested macro-and microplastics. *Remote Sens. Environ.* **2018**, *205*, 224–235. [CrossRef]
25. Papachristopoulou, I.; Filippides, A.; Fakiris, E.; Papatheodorou, G. Vessel-based photographic assessment of beach litter in remote coasts. A wide scale application in Saronikos Gulf, Greece. *Mar. Pollut. Bull.* **2020**, *150*, 110684. [CrossRef]
26. Martin, C.; Parkes, S.; Zhang, Q.; Zhang, X.; McCabe, M.F.; Duarte, C.M. Use of unmanned aerial vehicles for efficient beach litter monitoring. *Mar. Pollut. Bull.* **2018**, *131*, 662–673. [CrossRef]

27. Kylili, K.; Kyriakides, I.; Artusi, A.; Hadjistassou, C. Identifying floating plastic marine debris using a deep learning approach. *Environ. Sci. Pollut. Res.* **2019**, *26*, 17091–17099. [CrossRef]
28. Geraeds, M.; van Emmerik, T.; de Vries, R.; bin Ab Razak, M.S. Riverine Plastic Litter Monitoring Using Unmanned Aerial Vehicles (UAVs). *Remote Sens.* **2019**, *11*, 2045. [CrossRef]
29. Bao, Z.; Sha, J.; Li, X.; Hanchiso, T.; Shifaw, E. Monitoring of beach litter by automatic interpretation of unmanned aerial vehicle images using the segmentation threshold method. *Mar. Pollut. Bull.* **2018**, *137*, 388–398. [CrossRef]
30. Deidun, A.; Gauci, A.; Lagorio, S.; Galgani, F. Optimising beached litter monitoring protocols through aerial imagery. *Mar. Pollut. Bull.* **2018**, *131*, 212–217. [CrossRef]
31. Fallati, L.; Polidori, A.; Salvatore, C.; Saponari, L.; Savini, A.; Galli, P. Anthropogenic Marine Debris assessment with Unmanned Aerial Vehicle imagery and deep learning: A case study along the beaches of the Republic of Maldives. *Sci. Total Environ.* **2019**, *693*, 133581. [CrossRef]
32. Aoyama, T. Extraction of Marine Debris in the Sea of Japan Using High-Spatial-Resolution Satellite Images. In Proceedings of the SPIE 9878, Remote Sensing of the Oceans and Inland Waters: Techniques, Applications, and Challenges, New Delhi, India, 4–7 April 2016. 987817 (7 May 2016). [CrossRef]
33. Qi, L.; Hu, C.; Mikelsons, K.; Wang, M.; Lance, V.; Sun, S.; Barnes, B.B.; Zhao, J.; Van der Zande, D. In search of floating algae and other organisms in global oceans and lakes. *Remote Sens. Environ.* **2020**, *239*, 111659. [CrossRef]
34. Bulgarelli, B.; Zibordi, G. On the detectability of adjacency effects in ocean color remote sensing of mid-latitude coastal environments by SeaWiFS, MODIS-A, MERIS, OLCI, OLI and MSI. *Remote Sens. Environ.* **2018**, *209*, 423–438. [CrossRef]
35. Biermann, L.; Clewley, D.; Martinez-Vicente, V.; Topouzelis, K. Finding Plastic Patches in Coastal Waters Using Optical Satellite Data. *Sci. Rep.* **2020**, *10*, 1–10. [CrossRef]
36. Pandžic, M.; Mihajlovic, D.; Pandžic, J.; Pfeifer, N. Assessment of the geometric quality of Sentinel-2 data. *ISPRS Int. Arch. Photogramm. Remote Sens. Spat. Inf. Sci.* **2016**, *XLI-B1*, 489–494. [CrossRef]
37. Vanhellemont, Q.; Ruddick, K. Remote Sensing of Environment Advantages of high quality SWIR bands for ocean colour processing: Examples from Landsat-8. *Remote Sens. Environ.* **2015**, *161*, 89–106. [CrossRef]
38. Vanhellemont, Q. Remote Sensing of Environment Adaptation of the dark spectrum fi tting atmospheric correction for aquatic applications of the Landsat and Sentinel-2 archives. *Remote Sens. Environ.* **2019**, *225*, 175–192. [CrossRef]
39. Vanhellemont, Q.; Ruddick, K. Remote Sensing of Environment Atmospheric correction of metre-scale optical satellite data for inland and coastal water applications. *Remote Sens. Environ.* **2018**, *216*, 586–597. [CrossRef]
40. Harmel, T.; Chami, M.; Tormos, T.; Reynaud, N.; Danis, P.-A. Sunglint correction of the Multi-Spectral Instrument (MSI)-SENTINEL-2 imagery over inland and sea waters from SWIR bands. *Remote Sens. Environ.* **2018**, *204*, 308–321. [CrossRef]
41. Kokaly, R.F.; Clark, R.N.; Swayze, G.A.; Livo, K.E.; Hoefen, T.M.; Pearson, N.C.; Wise, R.A.; Benzel, W.M.; Lowers, H.A.; Driscoll, R.L.; et al. *USGS Spectral Library Version 7*; U.S. Geological Survey: Reston, VA, USA, 2017.
42. Harsanyi, J.C.; Chang, C.-I. Hyperspectral image classification and dimensionality reduction: An orthogonal subspace projection approach. *IEEE Trans. Geosci. Remote Sens.* **1994**, *32*, 779–785. [CrossRef]
43. Stocker, A.D. Multi-dimensional signal processing for electro-optical target detection. In *Proceedings of the Signal and Data Processing of Small Targets 1990*; SPIE: Washington, DC, USA, 1990; p. 18.
44. Kay, S.; Hedley, J.; Lavender, S. Sun Glint Correction of High and Low Spatial Resolution Images of Aquatic Scenes: A Review of Methods for Visible and Near-Infrared Wavelengths. *Remote Sens.* **2009**, *1*, 697–730. [CrossRef]
45. Kremezi, M.; Karathanassi, V. Correcting the BRDF effects on Sentinel-2 ocean images. In Proceedings of the Seventh International Conference on Remote Sensing and Geoinformation of the Environment (RSCy2019), Paphos, Cyprus, 18–21 March 2019; Papadavid, G., Themistocleous, K., Michaelides, S., Ambrosia, V., Hadjimitsis, D.G., Eds.; SPIE: Paphos, Cyprus, 2019; p. 45.